Nonlinear Rotordynamics of a MDOF Rotor-Stator Contact System Subjected to Frictional and Gravitational Effects

Elijah Chipato, A D Shaw, M I Friswell

College of Engineering, Swansea University Bay Campus, Fabian Way, Crymlyn Burrows, Swansea SA1 8EN, UK

Abstract

Rotating machines are intrinsically susceptible to expensive and high-risk faults such as rotor-stator rub. During a rub event normal and tangential forces are generated by the contact and friction that cause wear at the contacting interfaces. In the present work, such forces are computed by assuming linear elastic contact and Coulomb friction at multiple interface locations. A finite element shaft-line model of a horizontally mounted rotor is used to demonstrate the approach and the model is reduced for computational efficiency. The modal assurance criterion is used to identify the linear modes that contribute to a given solution. It is observed that bouncing solutions exist with rotor-stator contact in complex machines that can be viewed as internal resonances involving a small number of modes. The responses can become complex because different modes can combine to give the internal resonance (and hence a larger range of frequency ratios) and because of asymmetries, such as gravity. One design goal is to avoid any contact in the system and the analysis in this paper identifies the conditions for internal resonance that should be avoided in a real machine. The complicated dynamics shown here reveal some of the distinct features of contacting solutions and could also be used in condition monitoring to characterise faults.

Keywords: Friction, Gravity, Internal Resonance, Backward whirl, Modal Assurance Criterion

1. Introduction

The clearance between the stationary and rotating parts of a rotating machine has reduced in recent years, typically to increase the machine efficiency. Rotor-stator contact in these machines with small clearance becomes a critical fault; for example, aircraft engines have failed because of contact between the fan blade and the casing [1]. Rotor-stator contact has been studied for many years, usually for relatively simple systems. Johnson [2] studied a vertical shaft analytically

and determined the changes in synchronous whirl due a bearing with clearance. Choy *et al.* [3] investigated the effects of mass, support stiffness and blade stiffness during rotor stator rubbing for a simple rotor model, and showed intermittent behaviour and full rub. Ecker[4] investigated the steady state response of a rigid, single mass rotor supported by an active nonlinear magnetic bearing, and observed periodic, non-periodic and quasiperiodic solutions. Lawen and Flowers [5] studied the dynamic behaviour of a flexible rotor supported by linear bearings and an auxiliary bearing with clearance. Sinha [6] presented an analytical method to show the nonlinear dynamic effects of blades rubbing against a rigid outer case in rotating machinery. Smyth *et al.* [7] incorporated viscoelasticity into the stator support and investigated its effect on the global dynamics of a rotor-stator rub. Model order reduction methods have been suggested for high dimensional rotor systems [8, 9].

Asynchronous solutions have been identified in rotor-stator contact systems. Choi and Noah [10] viewed subharmonic frequency components as nonlinear resonant frequencies of the system. Ehrich [11] found that high speed rotors with bearing clearance exhibit high orders of subharmonic vibration particularly for systems with low damping and extreme nonlinearity. Childs [12] studied a Jeffcott model to explain the existence of (1/2)X and (1/3)X subharmonic motion in rotor systems with clearance. Childs [13] gave an explanation of the half frequency whirl for rotating machinery with light damping, and suggested the rub-induced whirl could be suppressed by lubricating the surfaces or reducing the local casing stiffness. Sun *et al.* [14] analysed a high speed rotor system with rub and observed periodic, chaotic and quasiperiodic solutions as the rotor spin speed increased. They observed two types of routes to chaos, namely the quasiperiodic route and the period doubling route.

The dynamics of a machine with rotor-stator contact has also been used for condition monitoring. Chu and Lu [15] assessed the feasibility to determine the rubbing location in a multi-disk rotor system by using dynamic stiffness identification. Liu *et al.* [16] proposed a method based on Nonlinear Output Frequency Response Functions to identify signal features; the method was verified with simulations and experiments. Hu *et al.* [17] conducted rub, crack and rub-crack coupled fault experiments and analysed the instantaneous frequency signatures of the faults using the Hilbert-Huang transform. The rub impact fault in rotating machines can cause periodic frequency modulation in the vibration response and Zhou *et al.* [18] used a fast modulated instantaneous frequency extraction to diagnose rubbing fault. Hong *et al.* [19] analysed the influence of rub on

the modal characteristics using the concept of complex nonlinear modes. It was observed that the modal frequencies of both the backward whirl (BW) and forward whirl (FW) modes increase with modal amplitude. The BW mode however sometimes became unstable. Mokhtar *et al.* [20] used the stator vibrations for rub identification instead of the rotor response which is normally difficult to measure.

In real machines BW motion is often destructive. Bartha [21] suggested to reduce the contact friction coefficient, to tune the dynamic properties of the stator and to reduce the coefficient of restitution of the impacts as methods to protect plants from BW. Fumagalli [22] found the whirl acceleration to be dependent on the material of the rotor and stator. Schmied and Pradetto [23] and Kirk *et al.* [24] considered the nonlinear dynamics following rotor drop to determine auxiliary bearings that inhibit the development of BW. Black [25] derived the existence condition of dry friction backward whirl (DFBW) using an unforced coupled nonlinear rotor/stator model and assuming pure rolling at the inception of DFBW. Ma *et al.* [26] considered the response due to a fan blade out event in an aero-engine, and showed that blade casing rubbing increases the resonance speed (resonance expansion). Bin *et al.* [27] investigated the dynamic response of a high speed turbocharger and observed that the subsynchronous 0.12X component caused rotor instability for small induced unbalance but as the unbalance is increased the vibration frequencies change from mainly 0.12X to synchronous vibration 1X. Nembhard *et al.* [28] conducted an experimental study on the shaft orbit response for different rotor related faults including rub. BW solutions were observed at subcritical speeds. Tehrani and Dardel [29] suggested using a tuned mass damper and a nonlinear energy sink to prevent contact. Bab *et al.* [30] modelled a two disk rotating machine and showed that a smooth nonlinear energy sink with rub at the disk positions can decrease the vibration and the inception of rub over a wide range of rotor spin speeds.

The motivation for this study comes from the work of Zilli *et al.* [31] who were the first to propose that the onset of bouncing type solutions can occur as a result of synchronisation of three fundamental frequencies, namely the rotor spin speed frequency, the FW frequency and the BW frequency. Shaw *et al.* [32, 33] suggested that this synchronisation may be interpreted as internal resonance. The resonance is caused by modal interaction of the FW and BW modes, and these solutions appear asynchronous in the stationary frame but periodic in the rotating frame. However, these studies do not address frictional and gravitational effects. The effect of gravity and friction on the internal resonance have been studied individually using a modified 2DOF Jeffcott rotor. For

the case with gravity, Chipato *et al.* [34] observed that gravity should be included for low shaft stiffness problems particularly for horizontal shaft systems but for high shaft stiffness, gravity can be ignored. Additional chaotic and multi periodic solutions, not seen for the case without gravity, were observed. Varney and Green [35] also highlighted that gravity has a significant impact on the non-linear response of rotor systems particularly at low rotor spin speeds which corresponds to the low stiffness case identified by [34]. For the case with friction, Chipato *et al.* [36] identified an additional type of quasiperiodic bouncing solution which was excited by friction and this was identified as the asynchronous periodic bouncing solution. A high amplitude response was also observed which proved to be a stiffened backward whirling (SBW) solution and as the coefficient of friction was increased the basin of attraction of this type of solution branch expanded. Crespo *et al.* [37] conducted an experiment to validate these internally resonating solutions. The experimental results lack the pristine geometrical elegance of a numerically simulated solution, however the presence of 2:1 frequencies and the higher orders visible in the solutions visualised in the rotating frame suggest that these solutions exist in reality. A good agreement between simulation and experiment was observed even though the numerical model did not include friction.

The focus of this study is the modal interaction which results in the onset of bouncing limit cycles. As discussed earlier, the effects of gravity and friction have been studied for a relatively simple 2DOF system with a single contact point. However, the influence of other modes in an MDOF system with multiple contacts is poorly understood, and this work intends to answer this question. In this work, a finite element shaft line model of a two disk rotor is developed, where the shaft comprises of Timoshenko beam elements. To make the analysis comprehensive, the study is done for both single contacts and double contacts. Studies are conducted on the effect of gravity, friction, coupled gravity and friction and finally the link between the gravitational and anisotropic case is discussed. The results are analysed using orbits and FFTs in both the stationary and rotating frames, bifurcation diagrams, spectral intensity plots and finally the modal assurance criterion (MAC) is used to reveal which modes contribute to a given solution.

The paper is organised as follows. Section 2 introduces the finite element model, the underlying assumptions and the final equations of motion. In Section 3 the modal assurance criterion (MAC) is discussed, which is used to determine the modal participation. Section 4 presents the results obtained from the numerical simulation and finally Section 5 gives the conclusions.

2. Finite Element Modelling

The Finite Element Method (FEM) is widely used in rotordynamics to develop the equations of motion of a given system [38]. The system under study in this work is shown in Figure 1. This

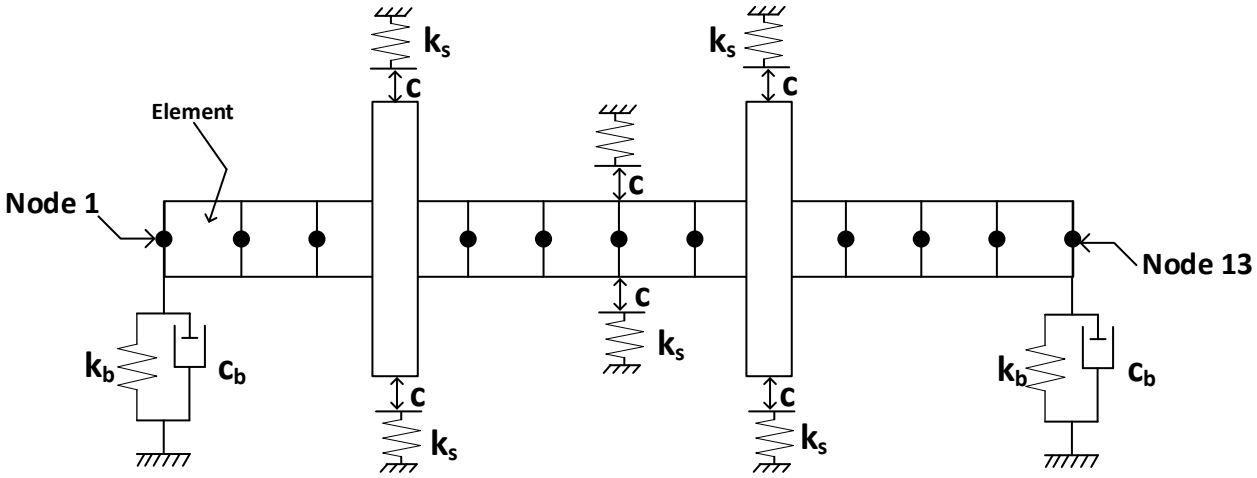

Figure 1: Schematic view of the rotor-bearing system, nodes, elements and potential contact locations.

system is the simplest machine that has multiple forward and backward whirling modes; since the arguments in the paper are based on the underlying linear modes of the machine, the proposed methods are easily applied to more complex machines. In order to study the rotor system, the FE model is simplified according to the following assumptions;

1. The right and left bearing are modelled as simple spring damper members of constant stiffness and damping unless mentioned that they are anisotropic.

2. The shaft is divided into 12 Timoshenko beam elements with 13 nodes. Each node has four degrees of freedom as shown in Figure 2, and therefore the entire system has 52 degrees of freedom (DOF). In Figure 2, x_i, y_i, θ_{yi} and θ_{xi} denote the displacements in translation and the angular displacements in the rotational direction of the i^{th} node

3. The two identical rigid disks are simulated as lumped mass elements superimposed on respective shaft nodes. These are simulated by the mass and the diametral and polar moments of inertia. The gyroscopic effects of the disks are also included. In Figure 2b, x_d, y_d, θ_{yd} and

θ_{xd} denote the displacements in translation and the angular displacements in the rotational direction of a disk member.

4. The rotor-stator contact is modelled by a clearance, c, and stator stiffness k_s. Although three positions of possible rotor-stator contact are shown in Figure 1, all of these locations are not implemented simultaneously.

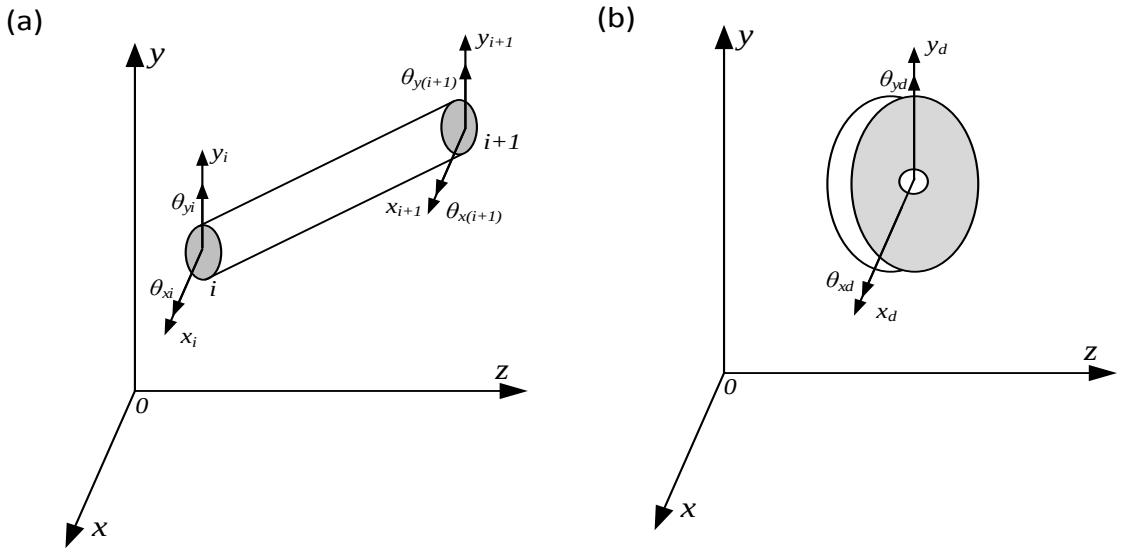

Figure 2: FE model of a Timoshenko shaft element and a rigid disk.

The general displacement vector of the two node shaft element can be expressed as;

$$\boldsymbol{q_j} = \begin{bmatrix} x_i & y_i & \theta_{xi} & \theta_{yi} & x_{i+1} & y_{i+1} & \theta_{x(i+1)} & \theta_{y(i+1)} \end{bmatrix}^T \tag{1}$$

where the subscript j denotes for the element number. The displacement vector of a rigid disk member $\boldsymbol{q}_k$ is

$$\boldsymbol{q}_k = \begin{bmatrix} x_d & y_d & \theta_{xd} & \theta_{yd} \end{bmatrix}^T \tag{2}$$

The stiffness, mass and gyroscopic matrices of the shaft and disk elements are represented by $\mathbf{K}_e$, $\mathbf{M}_e$, $\mathbf{G}_e$, $\mathbf{M}_d$, $\mathbf{G}_d$ and these are assembled to obtain the overall system. The assembled dynamic equation of motion of the rotor bearing system can be written as;

$$\mathbf{M}\ddot{\boldsymbol{q}} + (\Omega\mathbf{G} + \mathbf{C})\dot{\boldsymbol{q}} + \mathbf{K}\boldsymbol{q} = \mathbf{F}_u - \mathbf{F}_c - \mathbf{F}_g \tag{3}$$

where **K**, **M**, **G** and **C** are the stiffness, mass, gyroscopic and damping global matrices of the rotor bearing system. Ω is the rotor spin speed. In this work shaft damping is ignored and damping solely comes from the bearing supports. $\mathbf{F}_u$ is the excitation force due to the mass unbalance which only exists at the disk at node 4 and is given by;

$$\boldsymbol{F}_u = Re(\Omega^2 \boldsymbol{b_u} e^{i\Omega t}) \tag{4}$$

where $\boldsymbol{b_u}$ is the unbalance magnitude vector given by the product of the mass of the disk and its disk offset, ε and t is the time. The vector has two non-zero terms at the degrees of freedom of the disk where the unbalance excitation is imposed. $\mathbf{F}_g$ is the rotor system gravity and is given by

$$\boldsymbol{F}_g = \mathbf{M}\mathbf{g} \tag{5}$$

where **M** is the mass matrix and **g** is the gravity vector, $\mathbf{g} = \begin{bmatrix} 0 & -g & 0 & 0 & 0 & -g & 0 & 0... \end{bmatrix}^T$ where g is the acceleration due to gravity which is applied on every y_i degree of freedom along the rotor system [39]. $\mathbf{F}_c$ denotes the nonlinear contact force generated when the response, $r{=}\sqrt{x^2+y^2}$ of the machine exceeds the clearance. The undisturbed rotor of radius R is shown in Figure 3a where

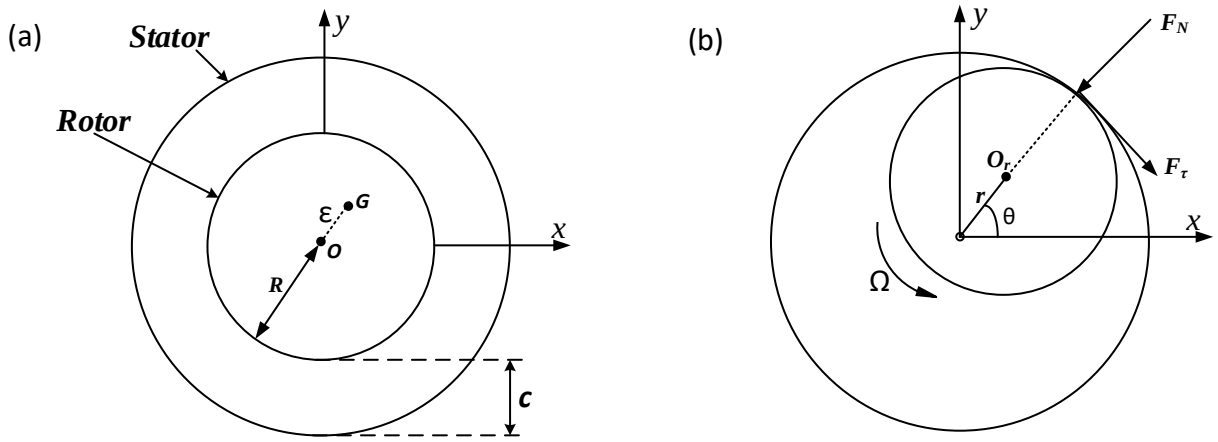

Figure 3: Undeflected rotor and deflected rotor with contact.

the geometric centre O_r is initially at the location O. During contact an elastic normal force, F_N, and a tangential force, F_τ, are generated at the interface as shown in Figure 3b. The elastic restoring force is linearly proportional to the interference by the stator stiffness k_s, meanwhile the tangential force is proportional to the product of the normal force, F_N and the coefficient of friction, μ. In

this study the Coulomb friction model is used. The contact force $\mathbf{F}_c$ is mathematically represented by the expression;

$$\boldsymbol{F}_{nl} = \begin{cases} k_s\left(1 - \frac{c}{r_c}\right)\begin{bmatrix} 1 & -\mu \\ \mu & 1 \end{bmatrix}\begin{Bmatrix} x_c \\ y_c \end{Bmatrix}, & \text{if } r \geq c \\ \begin{Bmatrix} 0 \\ 0 \end{Bmatrix}, & \text{if } r \leq c \end{cases} \tag{6}$$

$\mathbf{F}_{nl}$ is a 2-by-1 local vector with forces in the x and y directions, F_x and F_y. These are applied to the global contact force $\mathbf{F}_c$ which is a 52-by-1 matrix at the appropriate degrees of freedom. For this work, there can either be a single or double contact case. For the latter, one would have to compute the response at each contact location, here assumed at nodes 4 and 9, check whether the clearance has been exceeded and then apply the resulting contact forces to the DOF 13, 14, 33 and 34, ignoring the rotational degrees of freedom for each node. The symbols r_c, x_c and y_c are the local radial and lateral displacements at a contact location. The problem in this work has contact at either one or two nodes thus requiring a significant computational effort. For computational efficiency the model is reduced by only taking into account the first 8 mass normalized non-rotating modes. The simulations were performed and bifurcation plots obtained with 12 modes for typical cases to ensure that 8 modes was sufficient. The new transformed variable p is related to $\mathbf{U}$ by

$$\mathbf{q} = \mathbf{U}\mathbf{p} \tag{7}$$

where $\mathbf{U}$ is the 52-by-8 matrix of eigenvectors of the stationary system. The reduced mass, stiffness, damping and gyroscopic matrices are denoted $\mathbf{M}_r$, $\mathbf{K}_r$, $\mathbf{C}_r$ and $\mathbf{G}_r$. The relationship between the full and condensed matrices is

$$\begin{aligned} \mathbf{M}_r =& \mathbf{U}^T\mathbf{M}\mathbf{U} = \mathbf{I} \qquad \mathbf{G}_r = \mathbf{U}^T\mathbf{G}\mathbf{U} \\ \mathbf{K}_r =& \mathbf{U}^T\mathbf{K}\mathbf{U} = \mathbf{\Lambda}_r \qquad \mathbf{C}_r = \mathbf{U}^T\mathbf{C}\mathbf{U} \end{aligned} \tag{8}$$

where $\mathbf{I}$ is an 8-by-8 identity matrix and $\mathbf{\Lambda}_r$ is a diagonal matrix of the eigenvalues of the reduced system. Transforming Equation (3) into its condensed form gives

$$\ddot{\mathbf{p}} + \Omega(\mathbf{G}_r + \mathbf{C}_r)\dot{\mathbf{p}} + \mathbf{\Lambda}_r\mathbf{p} = \mathbf{U}^T(\mathbf{F}_u - \mathbf{F}_c - \mathbf{F}_g) \tag{9}$$

To solve Equation (9) it is convenient to write the equations in state space form as

$$\begin{Bmatrix} \dot{\mathbf{p}} \\ \dot{\mathbf{v}} \end{Bmatrix} = \begin{bmatrix} \mathbf{0} & \mathbf{I} \\ -\mathbf{\Lambda}_r & -(\mathbf{C}_r + \Omega\mathbf{G}_r) \end{bmatrix}\begin{Bmatrix} \mathbf{p} \\ \mathbf{v} \end{Bmatrix} + \begin{Bmatrix} \mathbf{0} \\ \mathbf{U}^T(\mathbf{F}_u - \mathbf{F}_c - \mathbf{F}_g) \end{Bmatrix} \tag{10}$$

These first order nonlinear equations can be numerically solved using an appropriate time integration solver. In this work the fourth order Runge Kutta procedure was used.

3. The Modal Assurance Criterion(MAC)

The Modal Assurance Criterion (MAC), also known as the Mode Shape Correlation Coefficient (MSCC), is a widely used statistical technique to estimate the degree of correlation between mode shape vectors[40–43]. Typically the MAC is used for comparison between measured and predicted mode shapes. Ewins [40] suggests that this statistical method is useful for all sorts of comparisons not only theory vs. experiment and that it can be applied to compare any pair of mode shape estimates. In this work the linear modes from the eigenvalue analysis are correlated with the nonlinear responses, in order to identify the modal content. Previous works, for example [32, 34, 36], rely on FFT observations to identify modal content, and this can require some interpretation due to nonlinearity causing response frequencies to shift from the underlying linear modal frequencies. However, since all of the responses are available at all of the degrees of freedom, one can use the MAC to perform a more rigorous identification of the participating modes. For each frequency peak in the FFT, one can get the complex FFT value which will give a vector of the response at that frequency. Also available are the complex modes at a given rotor spin speed from the eigenvalue analysis. With this information one can see which mode shape correlates best with the response frequencies, with the results presented in a bar chart or 2D table (similar to a MAC matrix in modal analysis). The correlation is easily performed using the scalar vector product normalised by the vector lengths as

$$MAC(l,n) = \frac{\mid \mathbf{U}_l^{\mathsf{H}} \mathbf{U}_n \mid^2}{(\mathbf{U}_n^{\mathsf{H}} \mathbf{U}_n)(\mathbf{U}_l^{\mathsf{H}} \mathbf{U}_l)} \tag{11}$$

where $\mathbf{U}_l$ and $\mathbf{U}_n$ are the complex linear mode from the eigenvalue analysis and the decomposition of the nonlinear motion into deflection shapes at each frequency peak in the FFT respectively. The vectors on the right side of Equation (11) are complex and thus the transpose is represented by the Hermitian transpose, H. In the MAC plots the deflection shapes for each frequency peak are represented by the term Nonlinear Frequency Components (NFC). This scalar product is complex but the absolute value is real and the MAC values range between zero and one, similar to that

of the conventional MAC, with 1 indicating that the deflection shape at a given frequency fully matches the given mode shape. Previous authors such as [43, 44] have used the MAC to identify linear modal participation in nonlinear responses, but to the author's knowledge this is the first time that this has been used to explore rotor-stator contact responses.

4. Numerical Simulations and Discussions

The reduced equation of motion in state space form in Equation (10) was solved numerically using the 4th/5th order variable step Runge Kutta solver, ode45 in Matlab. Table 1 shows the

Table 1: The FEA model system parameters

Symbol	Parameter	Value	Unit
E	Young's modulus	211	GPa
G	Shear modulus	81.2	GPa
ρ	Material density	7800	kg/m^3
g	Acceleration due to gravity	9.81	m/s^2
D_s	Shaft diameter	0.02	m
D_d	Disks diameter	0.3	m
c_b	Bearing damping	5e3	N/(m/s)
k_b	Bearing stiffness	4e6	N/m
h	disk thickness	0.01	m
e	Unbalance offset	0.5e-3	m
c	Clearance	5e-3	m
k_s	Contact stiffness	4e6	N/m

system parameters of the FEA model under study. The simulation was run for 100s. The integration results for each rotor spin speed were output as a 16 element vector consisting of displacements and velocities for the first 8 modal variables. This was then converted back into the physical coordinates resulting in a 52-by-n vector where 52 is the number of degrees of freedom of the FEA model. Appropriate DOF are then selected for further study, for example for node 4, the x and y DOFs corresponds to the 13th and 14th DOF.

In this work, the nonlinear dynamics were analysed using bifurcation diagrams, spectral intensity plots, FFT spectra in both the rotating and stationary frames, complex FFTs and Poincaré maps. In summary, the bifurcation diagrams were plotted by sampling the last 100 forcing periods of a given solution in the steady state region over a range of parameter values. This gives a summary of the essential nonlinear dynamics of a system by observing the structure of the bifurcation diagram as a system parameter is changed. Since colour graphics are widely used nowadays, a 3D waterfall plot can be projected onto a 2D plot with the intensity of the colour representing the amplitude, forming the spectral intensity plot. The Poincaré map is the stroboscopic portrait of a given motion at specific times and contains information about periodicity, quasi-periodicity, chaos and bifurcations of the system's dynamics. The results of this work are given as follows: the effect of gravity and friction are discussed separately for cases with a single and double contact and finally the effect of coupling both friction and gravity is given.

4.1. The effect of gravity on the nonlinear rotor system

To illustrate the effect of gravity on the system, both the single contact and the double contact are analysed in this section. Figure 4 shows the bifurcation and spectral intensity plots for the system with a single contact at node 7 for the case with no gravity force (Figures 4a and 4c) and for the case with gravity (Figures 4b and 4d). For the spectral intensity plots, amplitudes that are greater than 0.5mm are shown as dark red. It is apparent from the bifurcation and spectral intensity plots the qualitative changes that happen upon introduction of asymmetry into the system. There is also a reduction in bouncing solutions upon introducing asymmetry to the system.

Furthermore, the bouncing solutions at higher rotor spin speeds, that is, in the neighbourhood of 7000rpm, seem to be unchanged by just looking at the spectra even though these have decreased in number as compared to the non-gravity case. To get more insight into the nature of the dynamics, orbits visualised both in the stationary and rotating frames and their respective FFTs are presented. The stationary frame orbits are superimposed with a Poincaré map of the given solution. Figures 5, 7 and 8 shows orbits and FFTs obtained for the zero gravity case at 3650rpm, 4430rpm and 6590rpm respectively. It is apparent from these plots that one striking feature they possess is the difference in the number of loops in the orbit that is visualised in the rotating frame. In Figure 5, for the FFT plot we see three major peaks for the motion in the stationary frame with one of them being the excitation frequency at 3650rpm. The origins of the remaining two peaks at 1776rpm

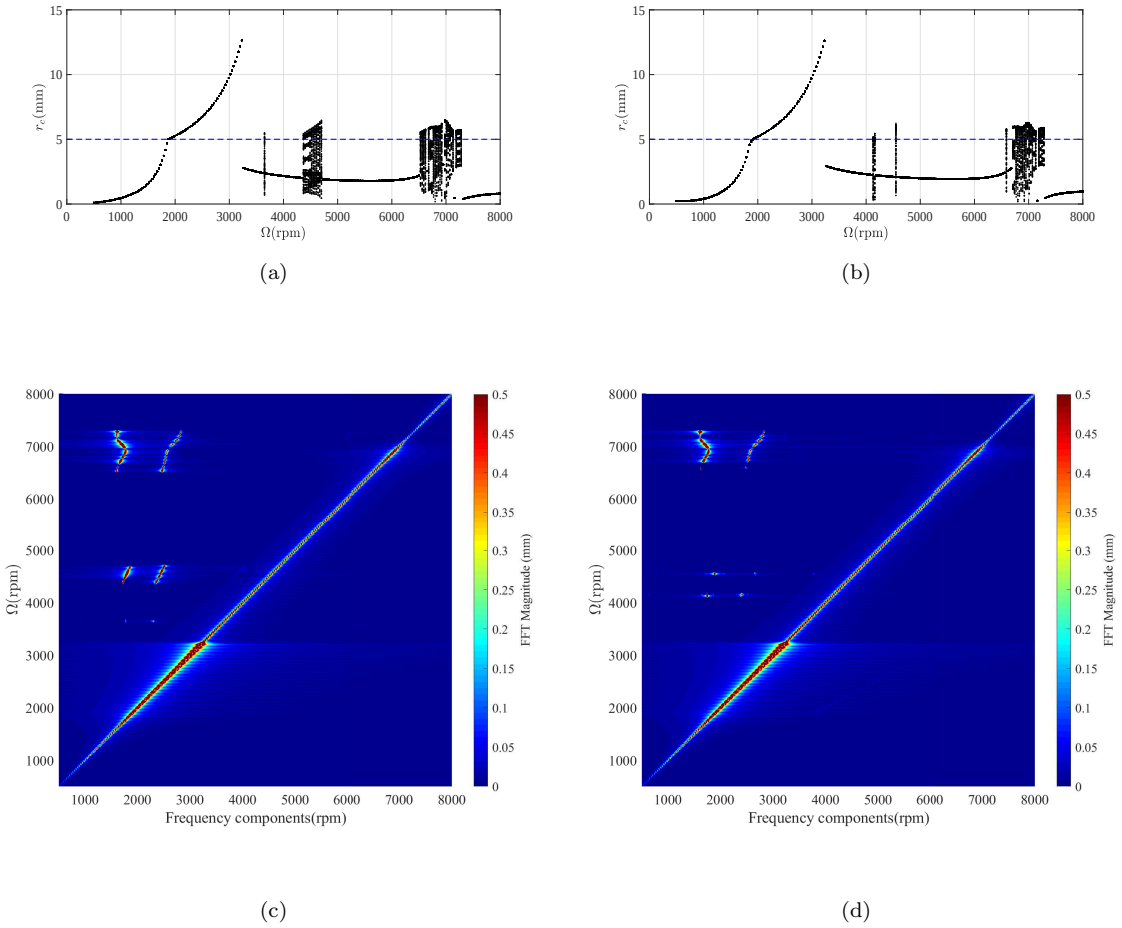

Figure 4: Bifurcation and spectral intensity plot for single contact at node 7, (4a and 4c) for the case with no gravity and (4b and 4d) for the case with gravity.

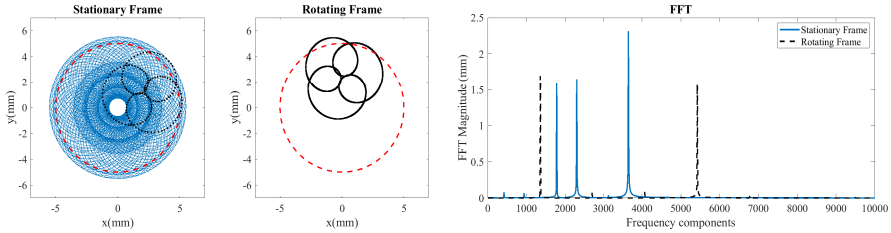

Figure 5: Orbits and FFTs visualised in both stationary and rotating frame at 3650rpm at node 7.

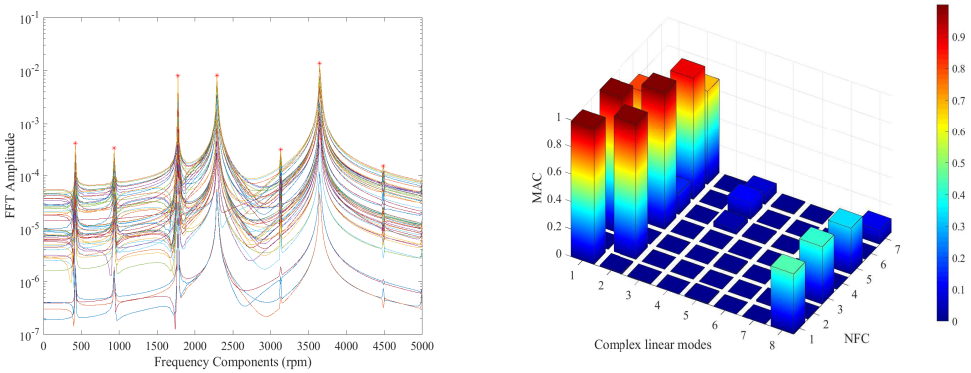

Figure 6: FFT for all degrees of freedom and the MAC for 3650rpm with contact at node 7.

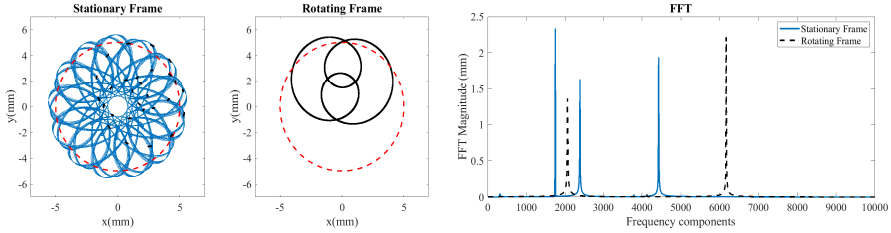

Figure 7: Orbits and FFTs visualised in both stationary and rotating frames at 4430rpm at node 7.

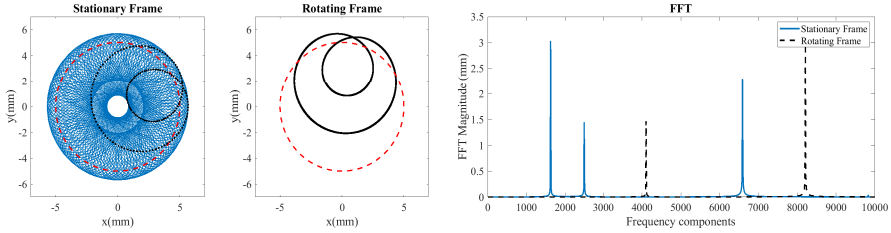

Figure 8: Orbits and FFTs visualised in both stationary and rotating frames at 6590rpm at node 7.

and 2292rpm can be obtained from the MAC calculation in Figure 6. The FFT plot shows the peaks used in the calculation of MAC and from the MAC calculation it is evident the modes which contribute to the existence of such a solution; these are the first BW and FW frequencies. The linear modal frequencies of these modes are 1723rpm and 2251rpm; these frequencies are lower than the ones obtained in the FFT because in contacting systems the linear modes tend to be stiffened. In addition, the nonlinear stiffened modal frequencies in the rotating frame are 1356rpm and 5424rpm; the two frequencies are in a ratio of 4:1, and this therefore makes this solution a 4:1

internal resonance solution.

Figure 7 shows the orbit and FFT at a higher speed of 4430rpm for the zero gravity case, where both the stationary and rotating frame orbits look strikingly different and in particular it is the rotating frame orbit with just two loops which is fewer than for the lower speed solution just discussed. The stationary frame FFT shares similar features to the one at a lower speed of 3650rpm with the three peaks representing the BW, FW and the excitation frequencies. The rotating frame FFT has peaks at 2052rpm and 6168rpm making this a 3:1 internal resonance solution. Figure

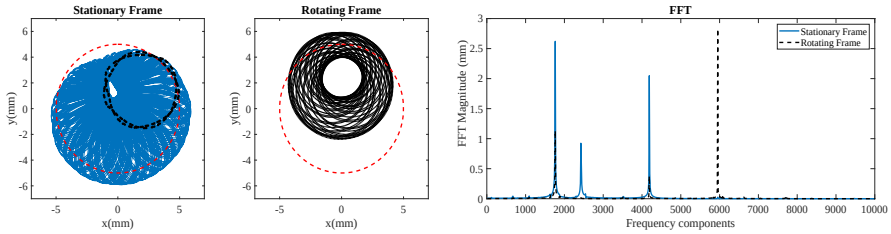

Figure 9: Orbits and FFTs visualised in both stationary and rotating frames at 4130rpm at node 7 for the case with gravity.

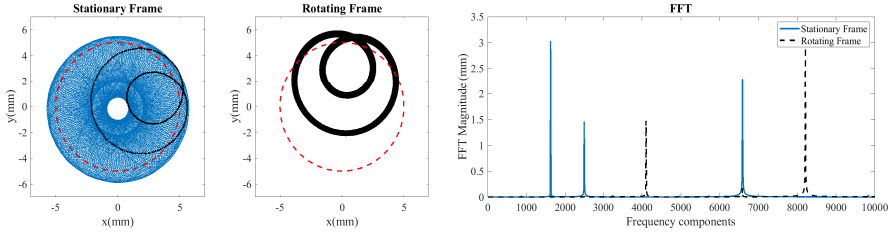

Figure 10: Orbits and FFTs visualised in both stationary and rotating frames at 6590rpm at node 7 for the case with gravity.

8 shows the orbits and FFTs at a much higher speed of 6590rpm for the zero gravity case. It is apparent that the rotating frame orbit has bifurcated into a single loop orbit. The stationary frame orbit has the typical three frequencies showing that the system is mode locked to give this type of internal resonance solution. Moreover, the rotating frame FFT shows peaks at 4104rpm and 8208rpm, and this is therefore a 2:1 internal resonance solution. It is therefore discernible from the zero gravity case results that the number of loops in the rotating frame can be used to predict the type of internal resonance solution; suppose L_n represents the number of loops in the rotating frame orbit then this will be an $(L_n + 1) : 1$ internal resonance solution.

Figures 9 and 10 shows orbits and FFTs for the case with gravity obtained at 4130rpm and 6590rpm. It is evident from the lower speed solution in Figure 9 that gravity induces asymmetry into the system as shown clearly in the stationary frame orbit which shows that the rotor precess in the lower part of the stator. This is solely an effect of very strong gravitational effects which results in directional stiffness variation. The orbit in the rotating frame shows a noisy circular orbit. The FFT in the stationary frame shows the typical three interacting frequencies at the BW, FW and excitation frequencies. The rotating frame FFT shows three peaks, the two shifted FW and BW frequencies and an attenuated peak at the rotor spin speed. It is also important to note that the FW in the rotating frame coincides in magnitude with the BW frequency in the stationary frame. Figure 10 shows the orbit and FFTs at 6590rpm for the case with gravity, which is the same speed as that shown in Figure 8 for the zero gravity case so a direct comparison can be made. Both the orbits and FFTs are similar but the rotating frame orbit seems to appear more noisy than the zero gravity case whilst keeping the same structure. This implies that even with imperfection the limit cycles found in the isotropic case still exist. It also shows that at higher speeds there is weaker directionality leading to a more symmetrical stationary frame orbit as the increased momentum of the rotor overcomes the strong gravitational effects.

Figure 11 shows the bifurcation and spectral intensity plots for the double contact case with contact locations at nodes 4 and 9 which are the locations of the two disks. The single and double contact case share a similar feature which is the reduction in the number of contacting solutions with the introduction of gravitational effects in the system. In addition, we see that for both cases at higher speeds the spectral intensity plots show a broadband response with finite spectra suggesting the presence of chaotic solutions in the system. Figure 12 shows orbits and FFTs at 4460rpm for the zero gravity case with double contact. The rotating frame orbit has two loops suggesting that this is 3:1 internal resonance solution which was confirmed by observing the rotating frame FFT. Figure 13 shows the orbit and FFT at a higher speed of 6110rpm for the double contact case with no gravity. The rotating frame orbit shows a structure that seems to suggest that this is an entrainment of the single loop orbits shown earlier and thus this is a 2:1 internal resonance solution. The ratio of the 2 major peaks in the rotating frame suggest that this is indeed a 2:1 internal resonance solution. Figure 14 shows the orbits and FFTs at 6110rpm for the double contact case and it follows from the single contact case that even in the presence of multiple contacts the isotropic assumption is reasonably robust in rotating systems.

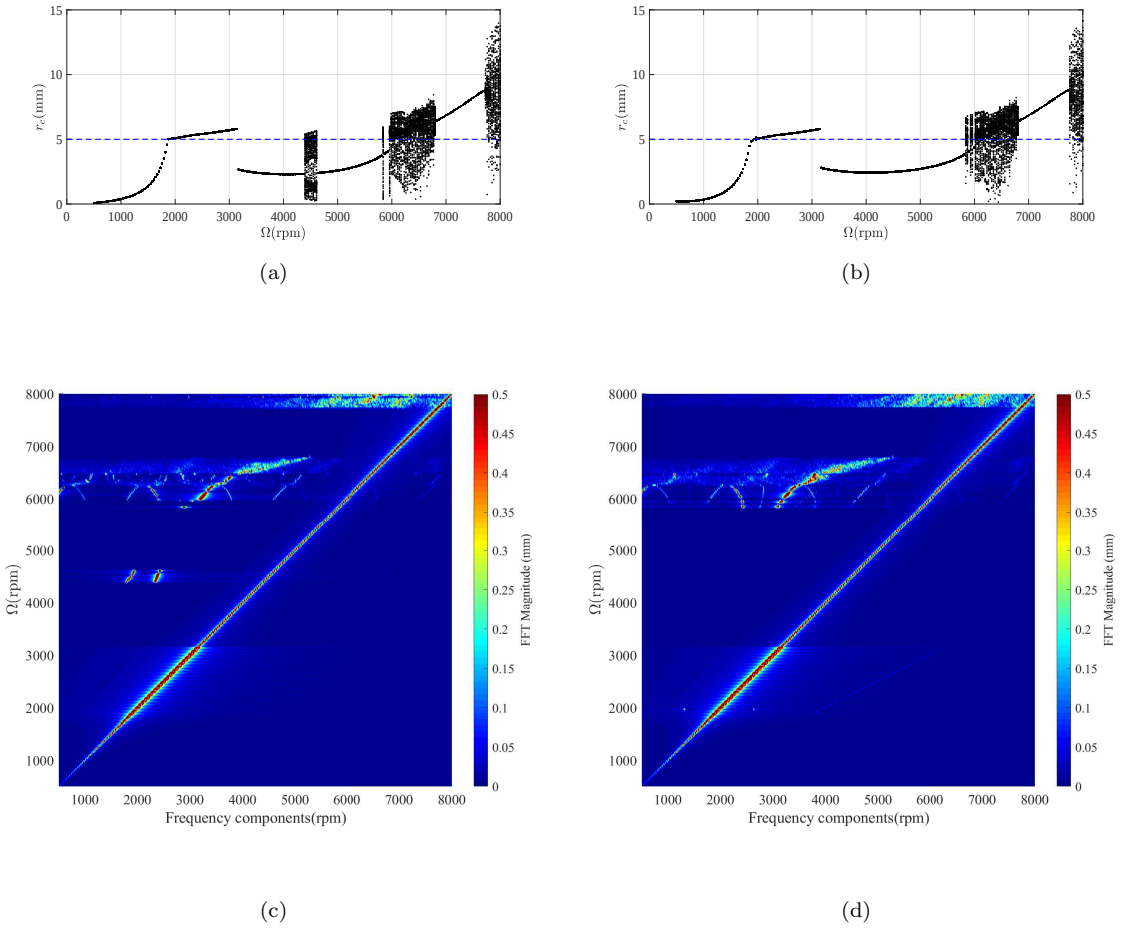

Figure 11: Bifurcation and spectral intensity plots for double contact at nodes 4 and 9. (11a and 11c) for the case with no gravity and (11b and 11d) for the case with gravity.

Rotor systems are usually supported by bearings and fluid film elements with anisotropic or asymmetric stiffness. One way of introducing anisotropy has already been discussed and this is the inclusion of gravity. Another way would be to have anisotropic bearings. Figures 15 and 16 shows orbits and stationary frame FFTs for the single and double contact cases at 7400rpm and 6800rpm respectively. The similarity in the solutions for both the single and double contact cases suggest that the inclusion of gravity to a system can be seen as similar to other forms of anisotropy.

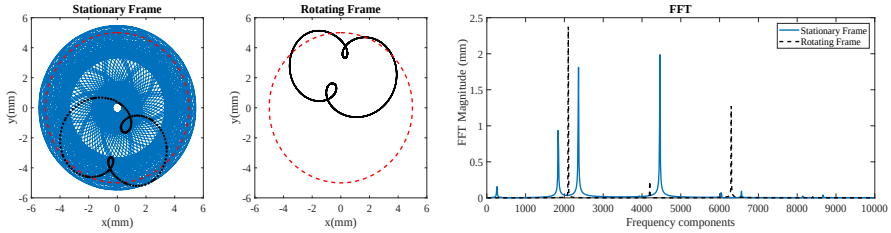

Figure 12: Orbits and FFTs visualised in both stationary and rotating frames for the double contact case(nodes 4 and 9) at 4460rpm at node 9.

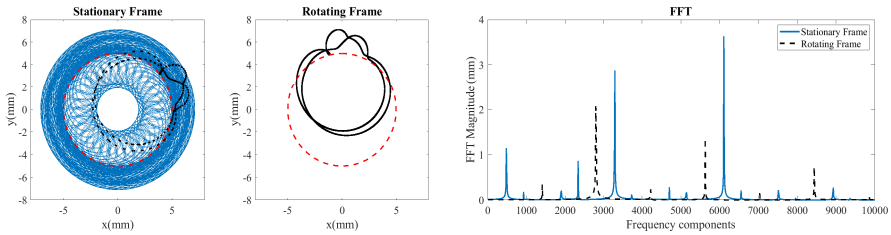

Figure 13: Orbits and FFTs visualised in both stationary and rotating frames for the double contact case(nodes 4 and 9) at 6110rpm at node 9.

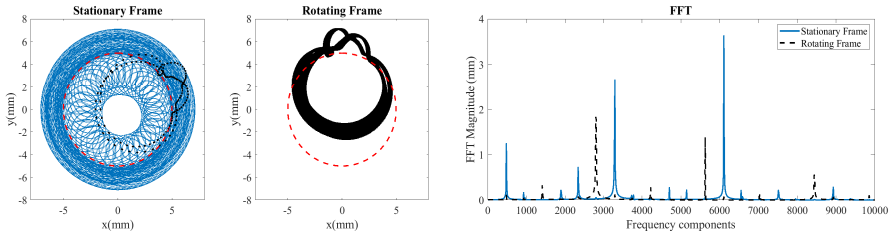

Figure 14: Orbits and FFTs visualised in both stationary and rotating frames for the double contact case(nodes 4 and 9) at 6110rpm at node 9 for the case with gravity.

4.2. The effect of friction on the nonlinear rotor system

Figure 17 shows the spectral intensity plots for a single contact at node 7 with friction in Figure 17a and for a double contact with contact locations at nodes 4 and 7 in Figure 17b. It is apparent from the two plots that the double contact case shows evidence of richer dynamics as compared to that of the single contact case. Also the introduction of friction into the system seems to excite complicated dynamics in the vicinity of the resonance expansion region close to the first natural frequency of the system. Figure 18 shows the orbits and FFTs for a typical solution in the resonance expansion region of the first natural frequency of the system. The rotating frame orbit

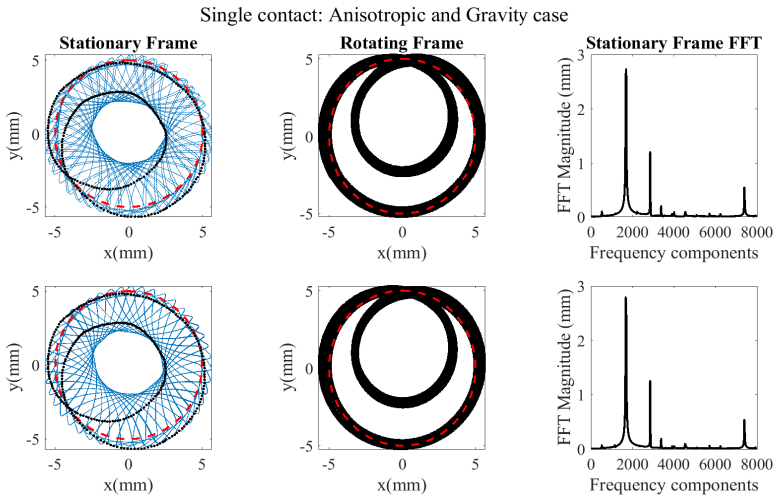

Figure 15: Comparison of orbits and FFTs for the anisotropic($k_x = 4e6$, $k_y = 3.9e6$) and gravity case at 7400rpm.

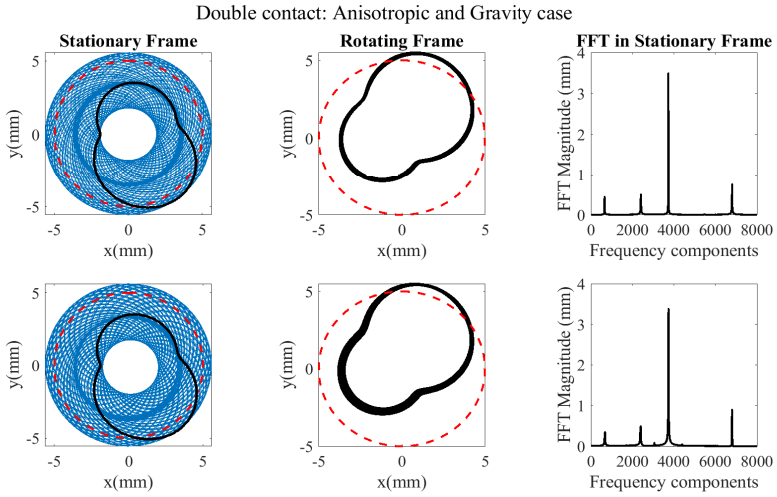

(a)

Figure 16: Comparison of orbits and FFTs for the anisotropic($k_x = 4e6$, $k_y = 3.9e6$) and gravity case at 6800rpm.

clearly shows that this is a periodic bouncing solution as it shows a circular orbit and a single peak in the rotating frame which is the sum of the two peaks in the stationary frame. The two peaks therefore corresponds to the excitation frequency and the contact frequency. These types of orbits are thereby referred to as Friction Induced Asynchronous Partial Contacting solutions. Figure

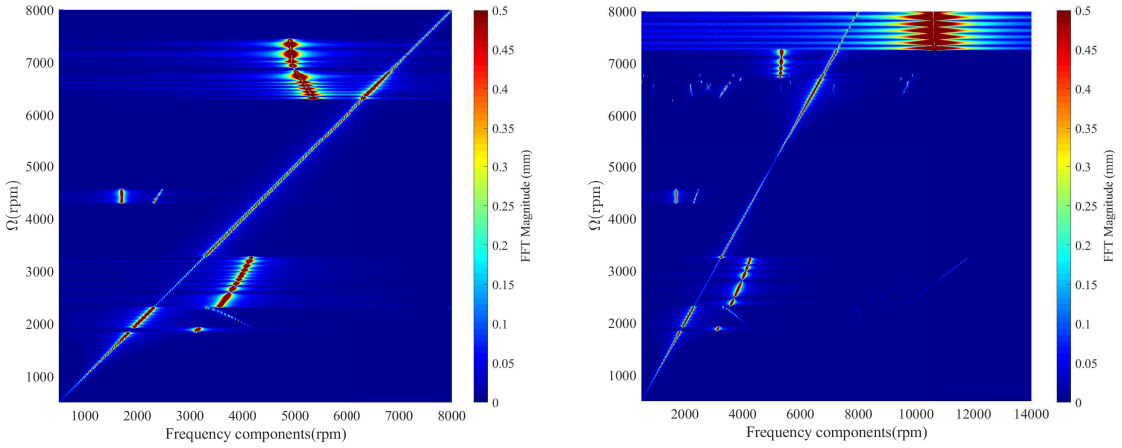

Figure 17: Spectral intensity plots for a single contact at node7 in 17a and a double contact at nodes 4 and 7 in 17b for μ=0.1.

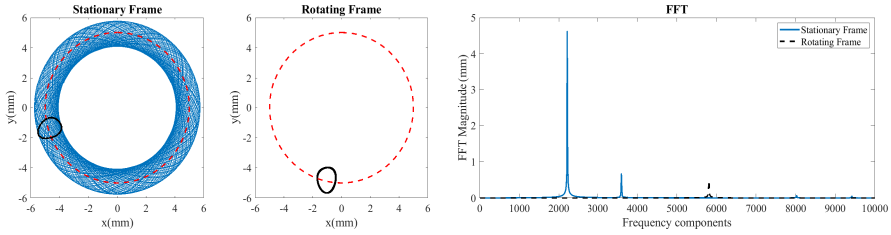

Figure 18: Orbits and FFTs visualised in both stationary and rotating frames for the single contact case(node 7) with friction at 2210rpm.

19 shows the MAC calculation showing the modes that are responsible for the existence of these friction induced asynchronous partial contacting solutions. Clearly, modes 1, 2 and 7 contribute the most, with modes 1 and 7 being the BW modes and they appear mainly because this solution is excited in the presence of friction. The FW mode here is excited mainly because the excitation frequency of 2210rpm is quite close to the first FW natural frequency which is at 2119rpm. Figure 20 shows a solution at 4430 rpm which has two loops in the rotating frame. The FFT in the rotating frame also shows that this is a 3:1 internal resonance solution and henceforth these types of solution

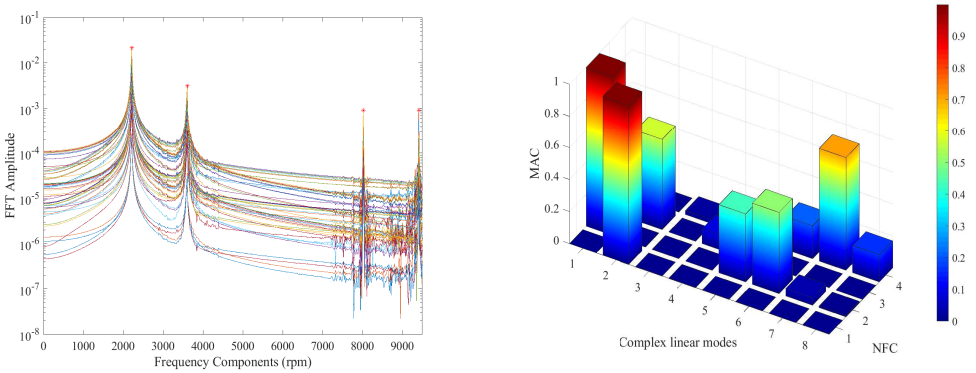

Figure 19: FFT for all degrees of freedom and the MAC for 2210rpm with contact at node 7.

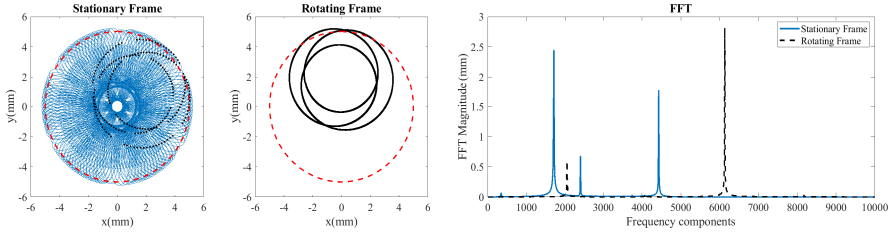

Figure 20: Orbits and FFTs visualised in both stationary and rotating frames for the single contact case(node 7) with friction at 4430rpm.

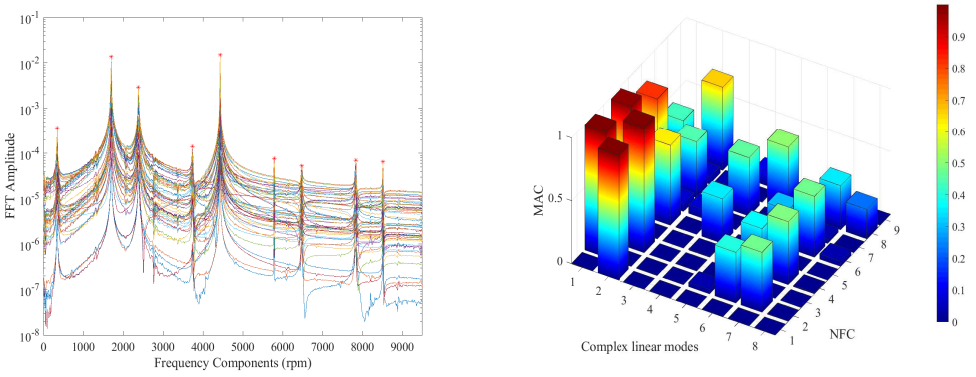

Figure 21: FFT for all degrees of freedom and the MAC for 4430rpm with contact at node 7.

are termed Internal Resonance Induced Partial contacting solutions. The MAC calculation shown in Figure 21 shows that the first BW and FW modes contribute the most to this solutions. The natural frequencies of these modes are 1652rpm and 2254rpm, and these approximately correspond

to the FFT values which are at 1702rpm and 2380rpm; the difference being due to the stiffening effect of the stator. The last type of solution is excited by friction; as shown in Figure 22. From

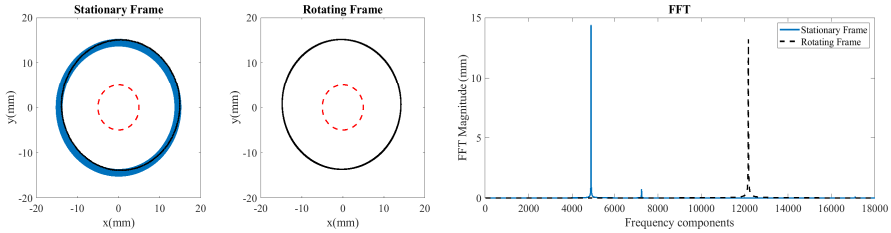

Figure 22: Orbits and FFTs visualised in both stationary and rotating frames for the single contact case(node 7) with friction at 7250rpm.

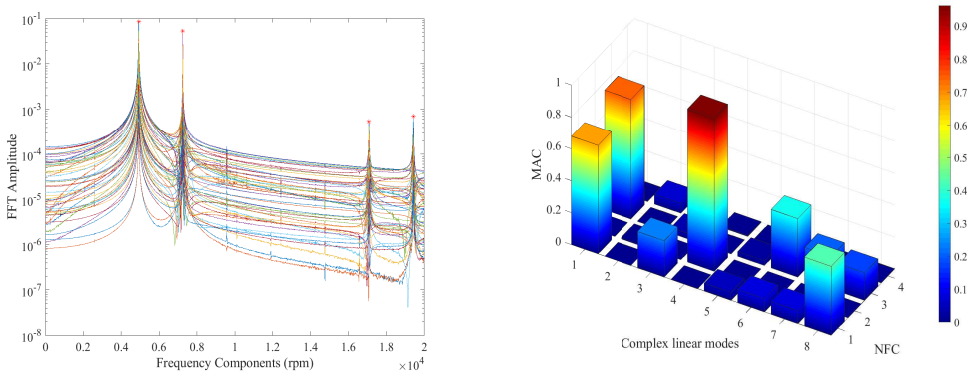

Figure 23: FFT for all degrees of freedom and the MAC for 7250rpm with contact at node 7.

the orbit in the stationary frame this is a very high amplitude solution and is in permanent contact with the stator. The stationary frame FFT consists of a highly attenuated excitation frequency and a second high magnitude peak which appears to be the BW frequency. The MAC calculation shows that the solution is dominated by mode 1 which is the first BW mode and mode 4 which is the second FW mode. The natural frequency of these modes are 1454rpm and 6888rpm; the FFT of the response has major peaks at 4926rpm and 7251rpm and clearly the second peak values somewhat matches but for the other peak the difference is large. However, since the rotor is in permanent contact the linear natural frequency would be significantly different to the FFT value and thus one has to calculate the stiffened natural frequencies which assume permanent contact at node 7; from this the new stiffened BW frequency was found to be 5260rpm. For the double contact

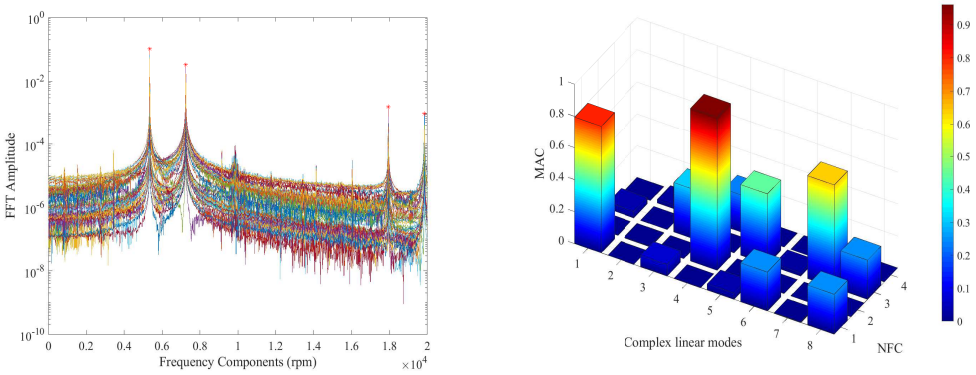

Figure 24: FFT for all degrees of freedom and the MAC for 7250rpm with contact at node 4 and 7.

case it follows that the partial contact solutions are a good match with no extra stiffening due to an extra contact location. By inspection of the bifurcation diagrams at the two contact locations, that is at nodes 4 and 7, the response is such that when a location is in contact at node 7, node 4 is not and thus no extra stiffening effect occurs. In contrast, for the BW solution, inspection of the bifurcation diagram shows that the node 7 response is much larger than the clearance, at node 4 the bifurcation diagram shows that the rotor will be grazing the stator or rather bouncing. This introduces a little more stiffening effect and will thus introduce new modal contributions to this solution. Figure 24 shows the MAC calculation at 7250rpm for the double contact case with contact locations at node 4 and node 7 and the extra contact seems to excite mode 7 which is the 4th BW natural frequency. Please note that this mode was not excited in the single contact case shown in Figure 23.

4.3. Effect of coupled friction and gravity on the nonlinear rotor system

Real systems experience both friction and the universal gravity force. This section demonstrates how coupling these two forces will change the nonlinear dynamics of the system under study. Figure 25 shows the spectral intensity plots for a single contact at node 7 with both gravity and friction included and for the double contact case with contact at the location of the discs at node 4 and 9. By inspecting the two plots for the single contact case it is evident that one type of solution is absent, that is the internal resonance induced partial contacting cycles. This suggest that the existence of this type of solution is also dependent upon the location of the contact under study, and the reason for this could be that the disk elements have high polar moment of inertia. Furthermore,

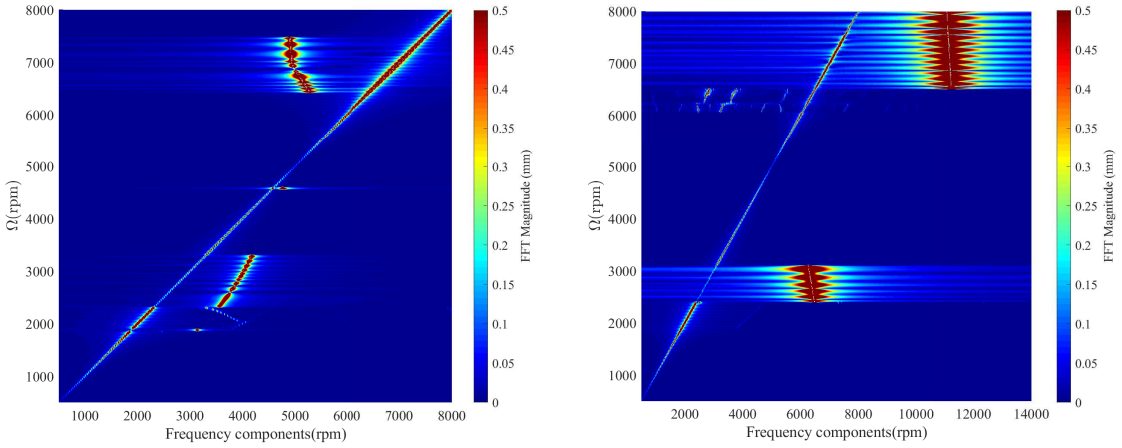

(a) (b)

Figure 25: Spectral intensity plots for a single contact at node7 in 25a and a double contact at nodes 4 and 9 in 25b for the case with friction (μ=0.1) and gravity.

the friction induced partial contacting cycles which have been seen earlier appear in the vicinity of the first natural frequency and persist in addition to the BW solutions. For the double contact case

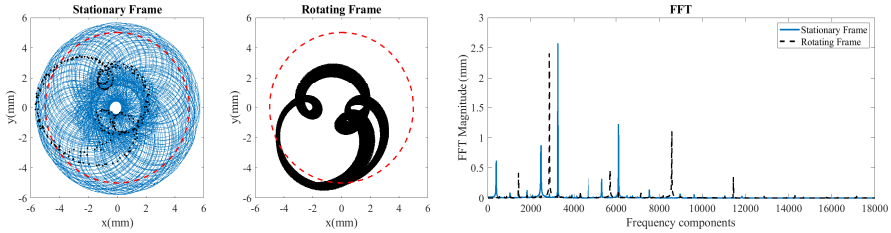

Figure 26: Orbits and FFTs visualised in both stationary and rotating frames at node 4 for the double contact case(nodes 4 and 9) with friction and gravity at 6110rpm.

with gravity and friction, friction induced asynchronous partial contacting cycles were observed. BW solutions were also observed but for this case the BW frequency was stiffened significantly more than the previous cases. On inspecting the bifurcation diagrams in these regions at nodes 4 and 9, the steady state response for both nodes was significantly more than the clearance thus the two

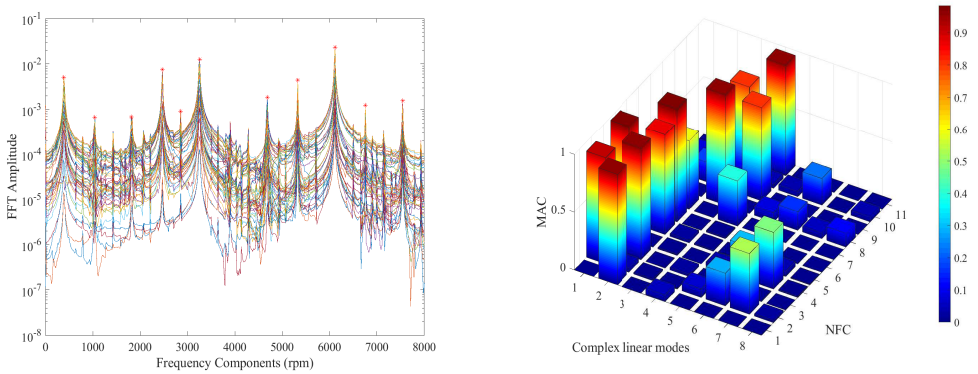

Figure 27: FFT for all degrees of freedom and the MAC for 6110rpm with contact at nodes 4 and 9.

contacts provided significant stiffening. In addition, it was also observed that there were several internal resonance induced partial contacting cycles and Figure 26 shows a typical solution at node 4. The two major peaks in the rotating frame FFT shows that this is a 3:1 internal resonance solution. The MAC calculation shown in Figure 27 shows that the first four modes contribute the most in this solution, and the natural frequencies of these modes are 1533rpm, 2345rpm, 5629rpm and 6854rpm. The four response frequencies correspond to 2449rpm, 3251rpm for the first BW and FW and these appear to be higher than the first two linear natural frequencies as a result of the stiffening effect due to the partial contacting behaviour. The last two natural frequencies correspond to 5328rpm and 6116rpm in the FFT; the second BW and FW appear to be lower than the FFT values with no stiffening. This is rather peculiar but could suggest an influence from other modes thereby causing an increased flexibility.

In light of the observed results it is apparent that this exercise has established with good confidence the effect of both gravitational and frictional forces on the synchronisation/ internal resonance phenomena which has been addressed here. The model used has its limitations, although for very short time impacts equivalent models can capture most of the effects, and very detailed models of the contact are beyond the scope of this paper. For example, a linear elastic contact model was used which is relatively simple to use as it includes only a few parameters. The set of parameters can be increased to include parameters such as wear at the contact interface, temperature dependencies of the rotor-stator contact interactions and contact damping.

5. Conclusion

In this paper an FEA model of a two disk rotor system with a single and double contact locations was used to analyse the nonlinear dynamics of the rotor with gravity, friction and with coupled gravity and friction. Bifurcation diagrams, orbits and spectral intensity plots were used to analyse the system. For the case with gravity it was observed that the internal resonance induced partial contacting cycles reduced with the introduction of gravity for both the single and double contact cases. It was evident that, for the single contact case, as the rotor spin speed increased the number of loops visible in the rotating frame decreased for the zero gravity case. It was also observed that very strong gravitational effects can lead to directional stiffness variation, however, at higher speed weaker directionality was observed leading to more symmetrical orbits in the stationary frame as the increase in momentum overcame the gravity.

For the double contact case at the location of the discs, the spectral intensity plots showed a broadband response with finite frequency peaks showing evidence of chaos. For the case with multiple contacts the limit cycles found in the isotropic case still exist. Also it was seen that the inclusion of gravity to the system can be viewed as similar to other forms of anisotropy as shown by the similarity in solutions for the different cases. For the case with friction the double contact case showed richer dynamics than the single contact case. Friction also excited complicated dynamics in the resonance expansion region for both the single and double contact cases. The BW frequency was also seen to be strongly dependent on whether there is permanent contact on both contact locations for the double contact case; if so, that meant stiffness will be significantly increased. The extra contact location also meant that new modal contributions would be excited. For the coupled gravity and friction case it was observed that the existence of certain types of solutions is dependent upon contact location. This is because a single contact location did not show evidence of internal resonance induced partial contacting cycles whereas the double contact case with coupled gravity and friction did. However, friction induced partial contacting cycles persisted. Finally, it was also observed that the influence of other modes caused extra flexibility and thus in some cases frequencies that were supposed to be stiffened were actually lower than expected.

The study conducted in this paper has provided significant insight into the features of the different solutions observed in practice. For example a noisy response in the rotating frame can show that gravity has a significant influence on the system dynamics and this information can be used in diagnostics to determine the root cause of certain observed dynamic behaviour. In

addition, the analysis can be used during the design stage of a machine. The goal is to avoid the possibility of bouncing solutions and at the design stage one would ensure that these solutions do not occur. Since this study has shown the modes which participate in an internal resonance, the designer could search for ways of modifying the rotating machine's properties to change the natural frequencies and avoid internal resonance within the operational rotor spin speed range of the machine. Alternatively, the designer could try and change the relative phasing of the mode shapes involved in internal resonance.

Acknowledgements

The research leading to these results has received funding from Swansea University via a ZCCE PhD scholarship.

References

[1] H. Ma, F. Yin, Y. Guo, X. Tai, B. Wen, A review on dynamic characteristics of blade–casing rubbing, Nonlinear Dynamics 84 (2016) 437–472.

[2] D. C. Johnson, Synchronous whirl of a vertical shaft having clearance in one bearing, Journal of Mechanical Engineering Science 4 (1962) 85–93.

[3] F. K. Choy, J. Padovan, J. C. Yu, Full rubs, bouncing and quasi chaotic orbits in rotating equipment, Journal of the Franklin Institute 327 (1990) 25–47.

[4] H. Ecker, Nonlinear stability analysis of a single mass rotor contacting a rigid backup bearing, in: V. I. Babitsky (Ed.), Dynamics of Vibro-Impact Systems, Springer, Berlin, Heidelberg, 1999, pp. 79–88. doi:10.1007/978-3-642-60114-9_9.

[5] J. L. Lawen, G. T. Flowers, Synchronous dynamics of a coupled shaft/bearing/housing system with auxiliary support from a clearance bearing: Analysis and experiment, J. Eng. Gas Turbines Power 119 (1997) 430–435.

[6] S. K. Sinha, Dynamic characteristics of a flexible bladed-rotor with coulomb damping due to tip-rub, Journal of Sound and Vibration 273 (2004) 875–919.

[7] P. A. Smyth, P. A. Varney, I. Green, A fractional calculus model of viscoelastic stator supports coupled with elastic rotor–stator rub, Journal of Tribology 138 (2016) 041101.

[8] Y. Jin, K. Lu, L. Hou, Y. Chen, An adaptive proper orthogonal decomposition method for model order reduction of multi-disc rotor system, Journal of Sound and Vibration 411 (2017) 210–231.

[9] K. Lu, Z. Lu, Y. Chen, Comparative study of two order reduction methods for high-dimensional rotor systems, International Journal of Non-Linear Mechanics 106 (2018) 330 – 334.

[10] S.-K. Choi, S. T. Noah, Mode-locking and chaos in a Jeffcott rotor with bearing clearances, J. Appl. Mech. 61 (1994) 131–138.

[11] F. F. Ehrich, High order subharmonic response of high speed rotors in bearing clearance, ASME J. Vib., Acoust., Stress, Reliab. Des 110 (1988) 9–16.

[12] D. W. Childs, Fractional-frequency rotor motion due to nonsymmetric clearance effects, J. Eng. Gas Turbines Power 104 (1982) 533–541.

[13] D. W. Childs, Rub-induced parametric excitation in rotors, J. Mech. Des. 101 (1979) 640–644.

[14] Z. Sun, J. Xu, T. Zhou, Analysis on complicated characteristics of a high-speed rotor system with rub-impact, Mechanism and Machine Theory 37 (2002) 659–672.

[15] F. Chu, W. Lu, Determination of the rubbing location in a multi-disk rotor system by means of dynamic stiffness identification, Journal of Sound and Vibration 248 (2001) 235–246.

[16] Y. Liu, Y. Zhao, J. Li, F. Xi, S. Yu, Y. Zhang, Research on fault feature extraction method based on NOFRFs and its application in rotor faults, Shock and Vibration 2019 (2019) 3524948.

[17] A. Hu, L. Xiang, Y. Zhang, Experimental study on the intrawave frequency modulation characteristic of rotor rub and crack fault, Mechanical Systems and Signal Processing 118 (2019) 209–225.

[18] P. Zhou, M. Du, S. Chen, Q. He, Z. Peng, W. Zhang, Study on intra-wave frequency modulation phenomenon in detection of rub-impact fault, Mechanical Systems and Signal Processing 122 (2019) 342–363.

[19] J. Hong, P. Yu, D. Zhang, Y. Ma, Nonlinear dynamic analysis using the complex nonlinear modes for a rotor system with an additional constraint due to rub-impact, Mechanical Systems and Signal Processing 116 (2019) 443–461.

[20] M. A. Mokhtar, A. K. Darpe, K. Gupta, Analysis of stator vibration response for the diagnosis of rub in a coupled rotor-stator system, International Journal of Mechanical Sciences 144 (2018) 392–406.

[21] A. R. Bartha, Dry friction backward whirl of rotors, Ph.D. thesis, ETH Zurich, 2000.

[22] M. A. Fumagalli, Modelling and measurement analysis of the contact interaction between a high speed rotor and its stator, Ph.D. thesis, ETH Zurich, 1997.

[23] J. Schmied, J. C. Pradetto, Behavior of a one ton rotor being dropped into auxiliary bearings, in: Proceedings, 3rd International Symposium on Magnetic Bearings, Technomic Publishing, Lancaster, PA, 1992, pp. 144–156.

[24] R. G. Kirk, E. E. Swanson, F. H. Kavarana, X. Wang, Rotor drop test stand for AMB rotating machinery, part 1 : Description of test stand and initial results, in: Proc. 4th Int. Symp. Magnetic Bearings, ETH Zurich, 1994, pp. 207–212.

[25] H. F. Black, Interaction of a whirling rotor with a vibrating stator across a clearance annulus, Journal of Mechanical Engineering Science 10 (1968) 1–12.

[26] Y. Ma, Y. Wang, J. Hong, Dynamic model and theoretical investigation for the fan-blade out event in the flexible rotor system of aero-engine, in: K. Cavalca, H. Weber (Eds.), IFToMM 2018: Proceedings of the 10th International Conference on Rotor Dynamics, 2019, pp. 18–33. doi:10.1007/978-3-319-99272-3_2.

[27] G.-F. Bin, Y. Huang, S.-P. Guo, X.-J. Li, G. Wang, Investigation of induced unbalance magnitude on dynamic characteristics of high-speed turbocharger with floating ring bearings, Chinese Journal of Mechanical Engineering 31 (2018) 88.

[28] A. D. Nembhard, J. K. Sinha, A. Yunusa-Kaltungo, Experimental observations in the shaft orbits of relatively flexible machines with different rotor related faults, Measurement 75 (2015) 320 – 337.

[29] G. G. Tehrani, M. Dardel, Mitigation of nonlinear oscillations of a jeffcott rotor system with an optimized damper and nonlinear energy sink, International Journal of Non-Linear Mechanics 98 (2018) 122 – 136.

[30] S. Bab, M. Najafi, J. F. Sola, A. Abbasi, Annihilation of non-stationary vibration of a gas turbine rotor system under rub-impact effect using a nonlinear absorber, Mechanism and Machine Theory 139 (2019) 379–406.

[31] A. Zilli, R. J. Williams, D. J. Ewins, Nonlinear dynamics of a simplified model of an overhung rotor subjected to intermittent annular rubs, Journal of Engineering for Gas Turbines and Power 137 (2015) 065001.

[32] A. D. Shaw, A. R. Champneys, M. I. Friswell, Asynchronous partial contact motion due to internal resonance in multiple degree-of-freedom rotordynamics, Royal Society Proceedings Part A 472 (2016) 20160303.

[33] A. D. Shaw, A. R. Champneys, M. I. Friswell, Normal form analysis of bouncing cycles in isotropic rotor stator contact problems, International Journal of Mechanical Sciences 155 (2019) 83–97.

[34] E. T. Chipato, A. D. Shaw, M. I. Friswell, Effect of gravity-induced asymmetry on the nonlinear vibration of an overhung rotor, Communications in Nonlinear Science and Numerical Simulation 62 (2018) 78–89.

[35] P. Varney, I. Green, Nonlinear phenomena, bifurcations, and routes to chaos in an asymmetrically supported rotor–stator contact system, Journal of Sound and Vibration 336 (2015) 207 – 226.

[36] E. T. Chipato, A. D. Shaw, M. I. Friswell, Frictional effects on the nonlinear dynamics of an overhung rotor, Communications in Nonlinear Science and Numerical Simulation 78 (2019) 104875.

[37] R. S. Crespo, A. D. Shaw, M. I. Friswell, A. R. Champneys, Experimental characterisation of asynchronous partially contacting motion in a multiple-degree-of-freedom rotor system, Mechanical Systems and Signal Processing 145 (2020) 106904.

[38] H. Nelson, J. McVaugh, The dynamics of rotor-bearing systems using finite elements, Journal of Engineering for Industry (1976).

[39] M. I. Friswell, J. E. T. Penny, S. D. Garvey, A. W. Lees, Dynamics of Rotating Machines, Cambridge University Press, 2010. doi:10.1017/cbo9780511780509.

[40] D. Ewins, Modal Testing: Theory, Practice and Application,, volume 171, Research Studies Press LTD., Baldock, Hertfordshire, England, 2000.

[41] M. I. Friswell, J. E. Mottershead, Finite element model updating in structural dynamics, volume 38, Springer Science & Business Media, 2013.

[42] M. Pastor, M. Binda, T. Harčarik, Modal assurance criterion, Procedia Engineering 48 (2012) 543–548.

[43] A. Chandrashaker, S. Adhikari, M. I. Friswell, Quantification of vibration localization in periodic structures, Journal of Vibration and Acoustics 138 (2016).

[44] A. Tatar, C. W. Schwingshackl, M. I. Friswell, Dynamic behaviour of three-dimensional planetary geared rotor systems, Mechanism and Machine Theory 134 (2019) 39–56.